Hindawi
Journal of Function Spaces
Volume 2022, Article ID 7525056, 16 pages
https://doi.org/10.1155/2022/7525056

Research Article

Cubic Trigonometric Hermite Interpolation Curve: Construction, Properties, and Shape Optimization

Juncheng Li and Chengzhi Liu

College of Mathematics and Finance, Hunan University of Humanities, Science and Technology, Loudi 417000, China

Correspondence should be addressed to Juncheng Li; lijuncheng82@126.com

Received 7 October 2022; Revised 11 November 2022; Accepted 5 December 2022; Published 21 December 2022

Academic Editor: Kwok-Pun Ho

Cubic Hermite interpolation curve plays a very important role in interpolation curves modeling, but it has three shortcomings including low continuity, difficult shape adjustment, and the inability to accurately represent some common engineering curves. We construct a cubic trigonometric Hermite interpolation curve to make up the three shortcomings of cubic Hermite interpolation curve once and for all. The cubic trigonometric Hermite interpolation curve not only inherits the features of cubic Hermite interpolation curve but also achieves C^2 continuity, has local and global adjustability, and can accurately represent elliptical arc, circular arc, quadratic parabolic arc, cubic parabolic arc, and astroid arc that often appear in engineering. In addition, we give the schemes for optimizing the shape of the cubic trigonometric Hermite interpolation curve based on internal energy minimization. The schemes include optimizing the shape of planar curve and spatial curve. Some modeling examples show that the proposed schemes are effective and the cubic trigonometric Hermite interpolation curve is more practical than cubic Hermite interpolation curve.

1. Introduction

It is well known that cubic Hermite interpolation curve [1] is a common model to construct interpolation curves in engineering, and it has been widely applied in practical engineering problems [2–5]. However, cubic Hermite interpolation curve has three shortcomings: the first is that it only achieves C^1 continuity, so it cannot meet some engineering problems with better requirements for smoothness; the second is that its shape would be fixed once the interpolation conditions are given, so it cannot meet some engineering problems requiring high flexibility in shape adjustment; the last is that it cannot accurately represent some common engineering curves. Some generalized Hermite interpolation curves have been presented to make up for these shortcomings, such as the rational Hermite interpolation curves with free parameters [6], the trigonometric Hermite interpolation curves with free parameters [7], the higher degree Hermite interpolation curves with free parameters [8–10], etc. Most of these curves can make up for one or two shortcomings of cubic Hermite interpolation curve.

In the recent years, trigonometric polynomials have received much attention within geometric modeling. Such as the trigonometric Bézier curves [11–14], the trigonometric B-spline curves [15–17], the trigonometric interpolation curves [18, 19], etc. The curves constructed in trigonometric polynomial space have broad application prospects in engineering. To make up the three shortcomings of cubic Hermite interpolation curve once and for all, the first purpose of this paper is to construct a generalized Hermite interpolation curve in cubic trigonometric polynomial space. After the new Hermite interpolation curve is constructed, a further problem arises: how to optimize the shape of the curve to meet some specific requirements? Indeed, shape optimization of parametric curves has attracted more and more attention in recent years. Various objective functions have been proposed to optimize the shape of parametric curves, among which the internal energy of curves is a widely used objective function. Generally, the internal energy of curves includes stretch energy, strain energy (also called bending energy), and curvature variation energy (often replaced by Jerk's energy), see [20–28]. This paper's second purpose is

to optimize the shape of the new Hermite interpolation curve by minimizing the internal energy.

The main contributions of this paper are as follows:

(a) We construct the generalized Hermite interpolation curve named CTHI curve in cubic trigonometric polynomial space. CTHI curve not only interpolates the points and the corresponding tangent vectors but also achieves C^2 continuity, has local and global adjustability, and can accurately represent elliptical arc, circular arc, quadratic parabolic arc, cubic parabolic arc, and astroid arc that often appear in engineering. In other words, CTHI curve not only inherits the features of cubic Hermite interpolation curve but also makes up for the three shortcomings of cubic Hermite interpolation curve once and for all

(b) We give the detailed construction process of CTHI curve, which can provide a valuable reference for the construction of other generalized Hermite interpolation curves

(c) We adopt the internal energy minimization to determine the optimal values of the free parameters contained in CTHI curve. The internal energy minimization methods include the cases of planar CTHI curve and spatial CTHI curve. The CTHI curves generated by minimizing the internal energy are satisfactory compared with the curves with inappropriate free parameters

The rest of this paper is organized as follows. In Section 2, we briefly review cubic Hermite interpolation curve. In Section 3, we give the specific construction process of CTHI curve. In Section 4, we present the properties of CTHI curve. In Section 5, we provide shape optimization methods of CTHI curve based on internal energy minimization. Finally, we give a brief conclusion in Section 6.

2. Review of Cubic Hermite Interpolation Curve

Given a series of points $\boldsymbol{p}_j$ together with the corresponding tangent vectors $\boldsymbol{m}_j (j = 0, 1, \cdots, n)$, cubic Hermite interpolation curve can be expressed by [1]

$$\boldsymbol{H}_i(t) = f_0(t)p_i + f_1(t)\boldsymbol{p}_{i+1} + g_0(t)\boldsymbol{m}_i + g_1(t)\boldsymbol{m}_{i+1}, i = 0, 1, \cdots, n-1, \tag{1}$$

where $0 \le t \le 1$, $f_j(t)$, and $g_j(t)(j = 0, 1)$ are blending functions which can be described as follows,

$$\begin{cases} f_0(t) = 1 - 3t^2 + 2t^3, \\ f_1(t) = 3t^2 - 2t^3, \\ g_0(t) = t - 2t^2 + t^3, \\ g_1(t) = -t^2 + t^3. \end{cases} \tag{2}$$

The blending functions expressed in Equation (2) have the following characteristics at the endpoints,

$$\begin{bmatrix} f_0(0) & f_1(0) & g_0(0) & g_1(0) \\ f_0(1) & f_1(1) & g_0(1) & g_1(1) \\ f_0'(0) & f_1'(0) & g_0'(0) & g_1'(0) \\ f_0'(1) & f_1'(1) & g_0'(1) & g_1'(1) \end{bmatrix} = \begin{bmatrix} 1 & 0 & 0 & 0 \\ 0 & 1 & 0 & 0 \\ 0 & 0 & 1 & 0 \\ 0 & 0 & 0 & 1 \end{bmatrix}. \tag{3}$$

Benefit from Equation (3), cubic Hermite interpolation curve expressed in Equation (1) satisfies that

$$\boldsymbol{H}_i(0) = \boldsymbol{p}_i, \boldsymbol{H}_i(1) = \boldsymbol{p}_{i+1}, \boldsymbol{H}_i'(1) = \boldsymbol{m}_{i+1}, \boldsymbol{H}_i'(0) = \boldsymbol{m}_i, i = 0, 1, \cdots, n-1. \tag{4}$$

Equation (4) shows that cubic Hermite interpolation curve interpolates the points $\boldsymbol{p}_j$ and the tangent vectors $\boldsymbol{m}_j$ $(j = 0, 1, \cdots, n)$. In addition, Equation (4) also shows that $\boldsymbol{H}_i^{(k)}(1) = \boldsymbol{H}_{i+1}^{(k)}(0)$, $k = 0, 1$, $i = 0, 1, \cdots, n-1$, which means cubic Hermite interpolation curve satisfies C^1 continuity.

As mentioned in Introduction, cubic Hermite interpolation curve has three shortcomings. To make up for these shortcomings once and for all, we construct a kind of generalized cubic Hermite interpolation curve in cubic trigonometric polynomial space in this paper.

3. Construction of Cubic Trigonometric Hermite Interpolation Curve

Cubic Hermite interpolation curve is defined in the polynomial space $\{1, t, t^2, t^3\}$. To make the constructed generalized Hermite interpolation curve can make up for the three shortcomings of cubic Hermite interpolation curve once and for all, we consider using the cubic trigonometric polynomial space $\{1, \sin(t), \cos(t), \sin^2(t), \sin^3(t), \cos^3(t)\}$ to instead of the polynomial space $\{1, t, t^2, t^3\}$. It should be noted that $\cos^2(t)$ is left out in the cubic trigonometric polynomial space because $\sin^2(t) + \cos^2(t) \equiv 1$, which can ensure that the base functions are linearly independent.

We need to construct cubic trigonometric blending functions first, denoted by $F_j(t)$ and $G_j(t)(j = 1, 2)$, and then can express the corresponding curve as follows:

$$\boldsymbol{TH}_i(t) = F_0(t)\boldsymbol{p}_i + F_1(t)\boldsymbol{p}_{i+1} + G_0(t)\boldsymbol{m}_i + G_1(t)\boldsymbol{m}_{i+1}, i = 0, 1, \cdots, n-1, \tag{5}$$

where $\boldsymbol{p}_j$ and $\boldsymbol{m}_j (j = 0, 1, \cdots, n)$ are given points and corresponding tangent vectors, respectively.

From Equation (5), we have

$$\boldsymbol{TH}_{i+1}''(0) = F_0''(0)\boldsymbol{p}_{i+1} + F_1''(0)\boldsymbol{p}_{i+2} + G_0''(0)\boldsymbol{m}_{i+1} + G_1''(0)\boldsymbol{m}_{i+2}, \tag{6}$$

$$\boldsymbol{TH}_i''\left(\frac{\pi}{2}\right) = F_0''\left(\frac{\pi}{2}\right)\boldsymbol{p}_i + F_1''\left(\frac{\pi}{2}\right)\boldsymbol{p}_{i+1} + G_0''\left(\frac{\pi}{2}\right)\boldsymbol{m}_i + G_1''\left(\frac{\pi}{2}\right)\boldsymbol{m}_{i+1}. \tag{7}$$

Because we hope the curve expressed in (5) can achieve C^2 continuity, it must satisfy that $\boldsymbol{TH}_i''(\pi/2) = \boldsymbol{TH}_{i+1}''(0)$. Then, from Equations (6) and (7), we obtain

$$F_0''\left(\frac{\pi}{2}\right) = 0, F_1''(0) = 0, G_0''\left(\frac{\pi}{2}\right) = 0, G_1''(0) = 0, F_0''(0) = F_1''\left(\frac{\pi}{2}\right), G_0''(0) = G_1''\left(\frac{\pi}{2}\right). \tag{8}$$

Thus, the blending functions $F_j(t)$ and $G_j(t)(j = 1, 2)$ need to have the characteristics expressed in Equation (8) in addition to the similar characteristics given by Equation (3).

We express $F_j(t)$ and $G_j(t)(j = 1, 2)$ as follows:

$$[F_0(t) \quad F_1(t) \quad G_0(t) \quad G_1(t)] = [1 \quad \sin(t) \quad \cos(t) \quad \sin^2(t) \quad \sin^3(t) \quad \cos^3(t)]M, \tag{9}$$

where M is an undetermined matrix expressed as

$$M = \begin{bmatrix} a_{11} & a_{12} & a_{13} & a_{14} \\ a_{21} & a_{22} & a_{23} & a_{24} \\ a_{31} & a_{32} & a_{33} & a_{34} \\ a_{41} & a_{42} & a_{43} & a_{44} \\ a_{51} & a_{52} & a_{53} & a_{54} \\ a_{61} & a_{62} & a_{63} & a_{64} \end{bmatrix}. \tag{10}$$

From Equation (9), we have

$$[F_0(0) \quad F_1(0) \quad G_0(0) \quad G_1(0)] = [1 \quad 0 \quad 1 \quad 0 \quad 0 \quad 1]M, \tag{11}$$

$$[F_0(\pi/2) \quad F_1(\pi/2) \quad G_0(\pi/2) \quad G_1(\pi/2)] = [1 \quad 1 \quad 0 \quad 1 \quad 1 \quad 0]M, \tag{12}$$

$$\left[F_0'(0) \quad F_1'(0) \quad G_0'(0) \quad G_1'(0)\right] = [0 \quad 1 \quad 0 \quad 0 \quad 0 \quad 0]M, \tag{13}$$

$$\left[F_0'(\pi/2) \quad F_1'(\pi/2) \quad G_0'(\pi/2) \quad G_1'(\pi/2)\right] = [0 \quad 0 \quad -1 \quad 0 \quad 0 \quad 0]M, \tag{14}$$

$$\left[F_0''(0) \quad F_1''(0) \quad G_0''(0) \quad G_1''(0)\right] = [0 \quad 0 \quad -1 \quad 2 \quad 0 \quad -3]M, \tag{15}$$

$$\left[F_0''(\pi/2) \quad F_1''(\pi/2) \quad G_0''(\pi/2) \quad G_1''(\pi/2)\right] = [0 \quad -1 \quad 0 \quad -2 \quad -3 \quad 0]M. \tag{16}$$

Because $F_j(t)$ and $G_j(t)(j = 1, 2)$ should have the similar characteristics given by Equation (3), then from Equations (11), (12), (13), and (14) we obtain

$$\begin{cases} a_{11} + a_{61} = 1, \\ a_{12} + a_{62} = 0, \\ a_{13} + a_{63} = 0, \\ a_{14} + a_{64} = 1, \\ a_{11} + a_{41} + a_{51} = 0, \\ a_{12} + a_{42} + a_{52} = 1, \\ a_{13} + a_{43} + a_{53} = -1, \\ a_{14} + a_{44} + a_{54} = 0, \\ a_{21} = 0, \quad a_{22} = 0, \quad a_{23} = 1, \quad a_{24} = 0, \\ a_{31} = 0, \quad a_{32} = 0, \quad a_{33} = 0, \quad a_{34} = -1. \end{cases} \tag{17}$$

Recall that $F_j(t)$ and $G_j(t)(j = 1, 2)$ should have the characteristics expressed in Equation (8), then from Equations (15) and (16) we obtain

$$\begin{cases} -a_{21} - 2a_{41} - 3a_{51} = 0, \\ -a_{32} + 2a_{42} - 3a_{62} = 0, \\ -a_{23} - 2a_{43} - 3a_{53} = 0, \\ -a_{34} + 2a_{44} - 3a_{64} = 0, \\ -a_{31} + 2a_{41} - 3a_{61} = -a_{22} - 2a_{42} - 3a_{52}, \\ -a_{33} + 2a_{43} - 3a_{63} = -a_{24} - 2a_{44} - 3a_{54}. \end{cases} \tag{18}$$

Note that M has twenty-four undetermined numbers, it is necessary to set two free parameters in these undetermined numbers because Equations (17) and (18) only have twenty-two equations in total. If we set $a_{61} = \alpha$ and $a_{63} = \beta$ as free parameters, $\alpha, \beta \in R$, then from Equations (17) and (18) we could obtain

$$M = \begin{bmatrix} 1-\alpha & 2(\alpha-1) & -\beta & \dfrac{6\beta-10}{3} \\ 0 & 0 & 1 & 0 \\ 0 & 0 & 0 & -1 \\ 3(\alpha-1) & 3(1-\alpha) & 3\beta-2 & 3(2-\beta) \\ 2(1-\alpha) & \alpha & 1-2\beta & \dfrac{3\beta-8}{3} \\ \alpha & 2(1-\alpha) & \beta & \dfrac{13-6\beta}{3} \end{bmatrix}. \tag{19}$$

By substituting Equation (19) into Equation (9), we can obtain the cubic trigonometric blending functions expressed

as

$$\begin{cases} F_0(t) = (1-\alpha) + 3(\alpha-1)S^2 + 2(1-\alpha)S^3 + \alpha C^3, \\ F_1(t) = 2(\alpha-1) + 3(1-\alpha)S^2 + \alpha S^3 + 2(1-\alpha)C^3, \\ G_0(t) = -\beta + S + (3\beta-2)S^2 + (1-2\beta)S^3 + \beta C^3, \\ G_1(t) = \frac{1}{3}\left(2(3\beta-5) - 3C + 9(2-\beta)S^2 + (3\beta-8)S^3 + (13-6\beta)C^3\right), \end{cases} \tag{20}$$

where $S \coloneqq \sin(t)$, $C \coloneqq \cos(t)$, $t \in [0, \pi/2]$, α and β are free parameters, $\alpha, \beta \in R$. Then, the cubic trigonometric Hermite interpolation curve expressed in Equation (5) is gotten naturally.

To make the free parameters α and β local, we rewrite Equation (20) as follows:

$$\begin{cases} F_{i,0}(t) = (1-\alpha_i) + 3(\alpha_i-1)S^2 + 2(1-\alpha_i)S^3 + \alpha_i C^3, \\ F_{i,1}(t) = 2(\alpha_{i+1}-1) + 3(1-\alpha_{i+1})S^2 + \alpha_{i+1}S^3 + 2(1-\alpha_{i+1})C^3, \\ G_{i,0}(t) = -\beta_i + S + (3\beta_i-2)S^2 + (1-2\beta_i)S^3 + \beta_i C^3, \\ G_{i,1}(t) = \frac{1}{3}\left(2(3\beta_{i+1}-5) - 3C + 9(2-\beta_{i+1})S^2 + (3\beta_{i+1}-8)S^3 + (13-6\beta_{i+1})C^3\right), \end{cases} \tag{21}$$

where $S \coloneqq \sin(t)$, $C \coloneqq \cos(t)$, $t \in [0, \pi/2]$, α_i, α_{i+1}, β_i and β_{i+1} are free parameters. Then, we get the definition of the cubic trigonometric Hermite interpolation curve.

Definition 1. Given a series of points $\boldsymbol{p}_j$ together with the corresponding tangent vectors $\boldsymbol{m}_j (j = 0, 1, \cdots, n)$, the cubic trigonometric Hermite interpolation curve (CTHI curve for short) is defined by

$$\boldsymbol{TH}_i(t) = F_{i,0}(t)\boldsymbol{p}_i + F_{i,1}(t)\boldsymbol{p}_{i+1} + G_{i,0}(t)\boldsymbol{m}_i + G_{i,1}(t)\boldsymbol{m}_{i+1}, \; i = 0, 1, \cdots, n-1, \tag{22}$$

where $0 \le t \le 1$, $F_{i,j}(t)$ and $G_{i,j}(t) (j = 0, 1)$ are the cubic trigonometric blending functions expressed in Equation (21).

Given the same endpoints and the corresponding tangent vectors, CTHI curve segments with different free parameters are shown in Figure 1.

4. Properties of CTHI Curve

4.1. Interpolation and Continuity

Theorem 2. *CTHI curve interpolates $\boldsymbol{p}_j$ and $\boldsymbol{m}_j (j = 0, 1, \cdots, n)$, and achieves C^2 continuity.*

Proof. By computing from Equations (21) and (22), we have

$$\begin{cases} \boldsymbol{TH}_i(0) = \boldsymbol{p}_i, \; \boldsymbol{TH}_i(\pi/2) = \boldsymbol{p}_{i+1}, \\ \boldsymbol{TH}_i'(0) = \boldsymbol{m}_i, \; \boldsymbol{TH}_i'(\pi/2) = \boldsymbol{m}_{i+1}, \\ \boldsymbol{TH}_i''(0) = (3\alpha_i - 6)p_i + (3\beta_i - 4)\boldsymbol{m}_i, \\ \boldsymbol{TH}_i''(\pi/2) = (3\alpha_{i+1} - 6)\boldsymbol{p}_{i+1} + (3\beta_{i+1} - 4)\boldsymbol{m}_{i+1}. \end{cases} \tag{23}$$

Equation (23) shows that CTHI curve interpolates the points $\boldsymbol{p}_j$ and the tangent vectors $\boldsymbol{m}_j (j = 0, 1, \cdots, n)$. In addition, Equation (23) also shows that $\boldsymbol{TH}_i^{(k)}(\pi/2) = \boldsymbol{TH}_{i+1}^{(k)}(0)$, $k = 0, 1, 2$, $i = 0, 1, \cdots, n-1$, which means CTHI curve achieves C^2 continuity. □

4.2. Shape Adjustability

Theorem 3. *For given $\boldsymbol{p}_j$ and $\boldsymbol{m}_j (j = 0, 1, \cdots, n)$, the shape of CTHI curve can be adjusted locally or globally.*

Proof. Equation (22) shows that CTHI curve is composed of n segments, and each segment contains four free parameters α_i, α_{i+1}, β_i, and β_{i+1}. When the points $\boldsymbol{p}_j$ and the tangent vectors $\boldsymbol{m}_j (j = 0, 1, \cdots, n)$ are kept unchanged, we can adjust the shape of the curve locally by altering the values of the four free parameters contained in each segment. It is easy to find that the α_i, $\beta_i (i = 0, n-1)$ affect the shape of one segment, and α_i, $\beta_i (i = 1, 2, \cdots, n-2)$ affect the shape of two segments.

If we set $\alpha_i = \alpha$, $\beta_i = \beta$, $i = 0, 1, \cdots, n$, CTHI curve only contains two free parameters α and β. When the points $\boldsymbol{p}_j$ and the tangent vectors $\boldsymbol{m}_j (j = 0, 1, \cdots, n)$ are fixed, we can adjust the shape of the curve globally by changing the values of α and β. □

Example 4. Given $\boldsymbol{p}_0 = (0, 0)$, $\boldsymbol{p}_1 = (1, 0)$, $\boldsymbol{p}_2 = (2, 0)$, $\boldsymbol{p}_3 = (3, 0)$, $\boldsymbol{p}_4 = (4, 0)$, $\boldsymbol{m}_0 = (0, 1)$, $\boldsymbol{m}_1 = (0, -1)$, $\boldsymbol{m}_2 = (0, 1)$, $\boldsymbol{m}_3 = (0, -1)$, $\boldsymbol{m}_4 = (0, 1)$.

The corresponding CTHI curve is composed of four segments. Figures 2 and 3 show the local and global adjustment of CTHI curve by modifying the values of the free parameters, respectively.

Example 5. Given $\boldsymbol{p}_0 = (-1/2, 0, 5/3)$, $\boldsymbol{p}_1 = (-2, 0, 1)$, $\boldsymbol{p}_2 = (-2, -5, 0)$, $\boldsymbol{p}_3 = (2, -5, 0)$, $\boldsymbol{p}_4 = (9/2, 0, 1)$, $\boldsymbol{p}_5 = (2, 0, 5/3)$, $\boldsymbol{p}_6 = (0, 0, 6)$, $\boldsymbol{p}_7 = (-1/2, 0, 5/3)$, $\boldsymbol{m}_0 = (-1, 0, -1/2)$, $\boldsymbol{m}_1 = (-3/4, -1/2, -1/2)$, $\boldsymbol{m}_2 = (2, -5/2, -1/2)$, $\boldsymbol{m}_3 = (13/4, 5/2, 1/2)$, $\boldsymbol{m}_4 = (0, 5/2, 5/6)$, $\boldsymbol{m}_5 = (-9/4, -1/2, 0)$, $\boldsymbol{m}_6 = (-5/4, 0, 0)$, $\boldsymbol{m}_7 = (-1, 0, -5/2)$.

The corresponding closed CTHI curve is composed of seven segments. Figures 4 and 5 show the local and global adjustment of CTHI curve by modifying the values of the free parameters, respectively.

4.3. Accurate Representation of Some Engineering Curves.

We consider using one segment of CTHI curve to represent some engineering curves.

4.3.1. Accurate Representation of Elliptical Arc and Circular Arc

Theorem 6. *Let $\boldsymbol{p}_i = (0, b)$, $\boldsymbol{p}_{i+1} = (a, 0)$, $\boldsymbol{m}_i = (a, 0)$, $\boldsymbol{m}_{i+1} = (0, -b)$, $ab \neq 0$, and $\alpha_i = \alpha_{i+1} = 5/3$, $\beta_i = \beta_{i+1} = 4/3$, the CTHI curve segment $\boldsymbol{TH}_i(t)$ accurately represents an elliptical arc as long as $a \neq b$ and a circular arc as long as $a = b$.*

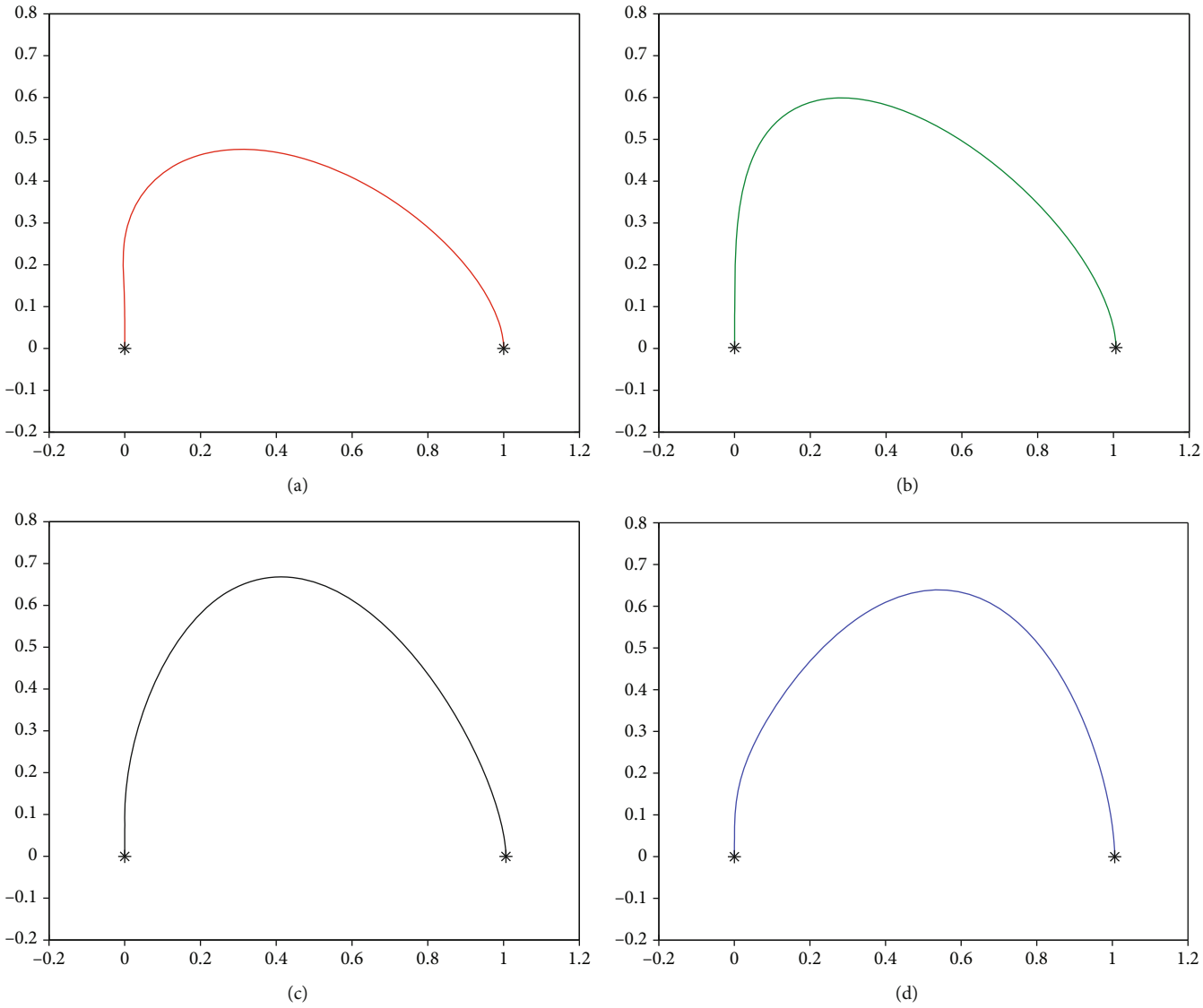

FIGURE 1: CTHI curve segments with different free parameters. (a) $(\alpha_i, \alpha_{i+1}, \beta_i, \beta_{i+1}) = (-1, -0.5, 0, 0.5)$. (b) $(\alpha_i, \alpha_{i+1}, \beta_i, \beta_{i+1}) = (-0.5, 0, 1, 0.5)$. (c) $(\alpha_i, \alpha_{i+1}, \beta_i, \beta_{i+1}) = (0.5, 0, -0.5, -1)$. (d) $(\alpha_i, \alpha_{i+1}, \beta_i, \beta_{i+1}) = (0.5, 1, 0, -0.5)$.

Proof. By substituting the given information into Equation (22), we have

$$\boldsymbol{TH}_i(t) = (a \sin(t), b \cos(t)), \tag{24}$$

where $t \in [0, \pi/2]$. Equation (24) is the exact expression of an elliptical arc as long as $a \neq b$ and is the exact expression of a circular arc as long as $a = b$, see Figure 6. □

4.3.2. Accurate Representation of Quadratic Parabolic Arc

Theorem 7. *Let* $\boldsymbol{p}_i = (-3a/4, -b/2)$, $\boldsymbol{p}_{i+1} = (a/4, b/2)$, $\boldsymbol{m}_i = (a, 0)$, $\boldsymbol{m}_{i+1} = (0, 0)$, $ab \neq 0$, *and* $\alpha_i = \alpha_{i+1} = 2/3$, $\beta_i = \beta_{i+1} = 1/3$, *the CTHI curve segment* $\boldsymbol{TH}_i(t)$ *accurately represents a quadratic parabolic arc.*

Proof. By substituting the given information into Equation (22), we have

$$\boldsymbol{TH}_i(t) = \left(-\frac{3a}{4} + a \sin(t), -\frac{b}{2} + b \sin^2(t)\right), \tag{25}$$

where $t \in [0, \pi/2]$. Equation (25) is the exact expression of a quadratic parabolic arc, see Figure 7. □

4.3.3. Accurate Representation of Cubic Parabolic Arc

Theorem 8. *Let* $\boldsymbol{p}_i = (-a/3, b)$, $\boldsymbol{p}_{i+1} = (2a/3, 0)$, $\boldsymbol{m}_i = (0, 0)$, $\boldsymbol{m}_{i+1} = (a, 0)$, $ab \neq 0$, *and* $\alpha_i = \alpha_{i+1} = 1$, $\beta_i = \beta_{i+1} = 2$, *the CTHI curve segment* $\boldsymbol{TH}_i(t)$ *accurately represents a cubic parabolic arc.*

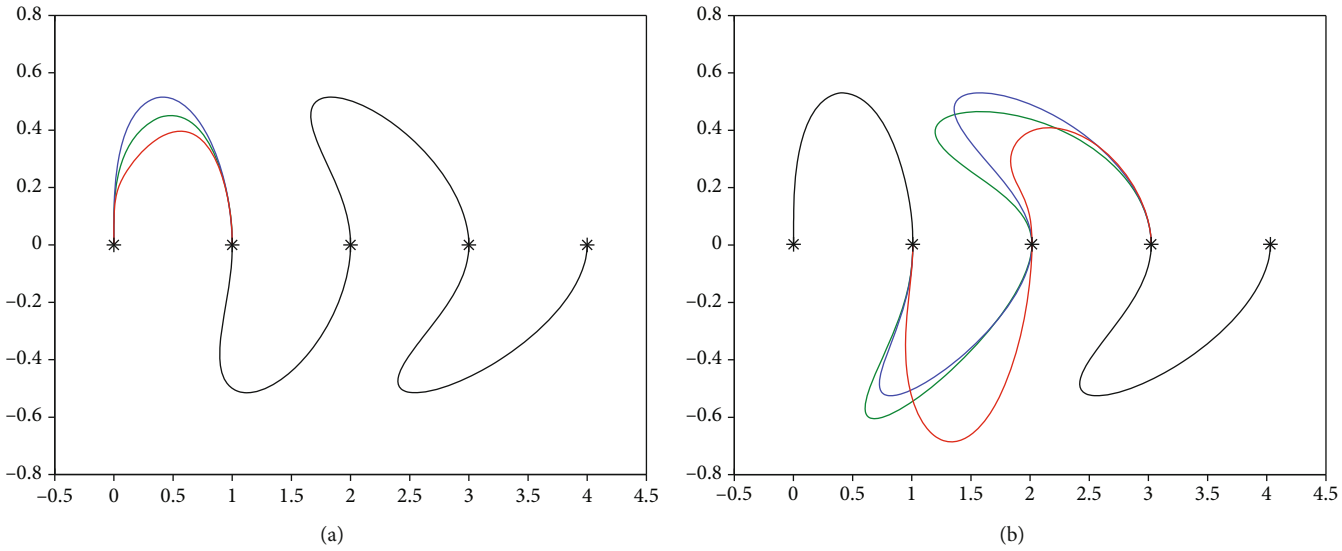

FIGURE 2: Local adjustment of planar CTHI curve. (a) $(\alpha_i, \beta_i) = (1, 1)(i = 1, 2, 3, 4)$, but $(\alpha_0, \beta_0) = (-0.5, 0.5)$ (green line), $(\alpha_0, \beta_0) = (0, 1)$ (blue line), $(\alpha_0, \beta_0) = (1.5, 0)$ (red line). (b) $(\alpha_i, \beta_i) = (1, 1)(i = 0, 1, 3, 4)$, but $(\alpha_2, \beta_2) = (-0.5, 0.5)$ (green line), $(\alpha_2, \beta_2) = (0, 1)$ (blue line), $(\alpha_2, \beta_2) = (1.5, 0)$ (red line).

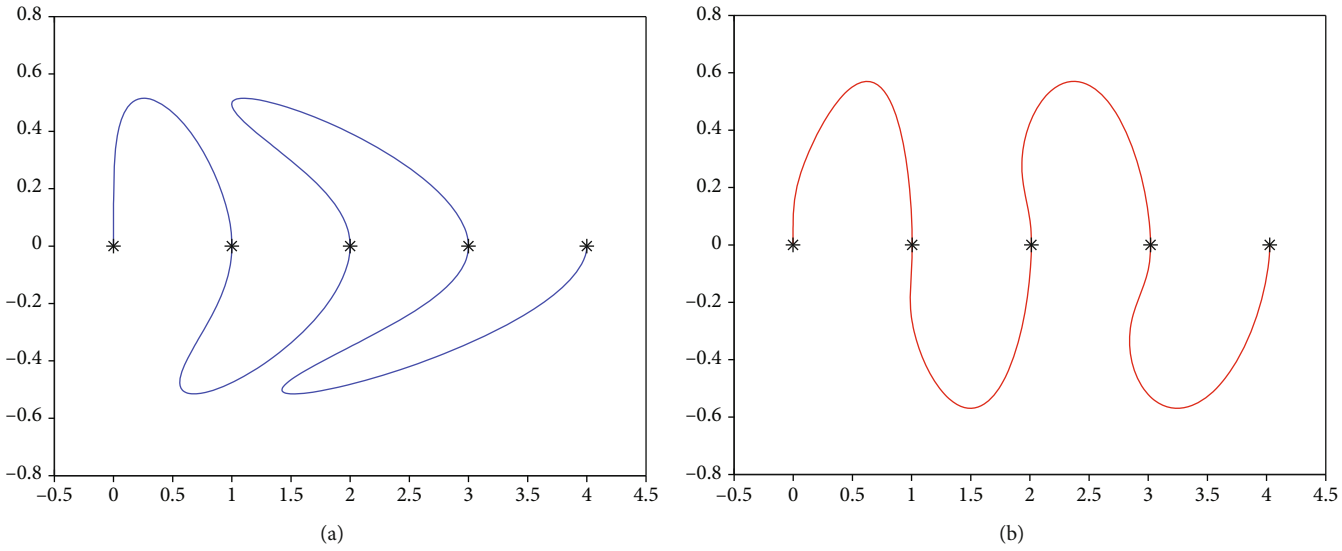

FIGURE 3: Global adjustment of planar CTHI curve. (a) $(\alpha, \beta) = (0, 1)$. (b) $(\alpha, \beta) = (1.5, 0)$.

Proof. By substituting the given information into Equation (22), we have

$$\boldsymbol{TH}_i(t) = \left(\frac{2a}{3} - a\cos(t), b\cos^3(t)\right), \tag{26}$$

where $t \in [0, \pi/2]$. Equation (26) is the exact expression of a cubic parabolic arc, see Figure 8. □

4.3.4. Accurate Representation of Astroid Arc

Theorem 9. *Let* $\boldsymbol{p}_i = (0, a)$, $\boldsymbol{p}_{i+1} = (a, 0)$, $\boldsymbol{m}_i = (0, 0)$, $\boldsymbol{m}_{i+1} = (a, 0)$, $a \neq 0$, *and* $\alpha_i = \alpha_{i+1} = 1$, $\beta_i, \beta_{i+1} \in R$, *the CTHI curve segment* $\boldsymbol{TH}_i(t)$ *accurately represents an astroid arc.*

Proof. By substituting the given information into Equation (22), we have

$$\boldsymbol{TH}_i(t) = \left(a\sin^3(t), a\cos^3(t)\right), \tag{27}$$

where $t \in [0, \pi/2]$. It is clear that Equation (27) is the exact expression of an astroid arc, see Figure 9. □

5. Shape Optimization of CTHI Curve Based on Internal Energy Minimization

As mentioned above, each segment of CTHI curve contains four free parameters α_i, α_{i+1}, β_i, and β_{i+1}. Although this will make the curve more flexible, it will also make the geometric operation more complex. We suggest taking $\alpha_i = \beta_i$ and

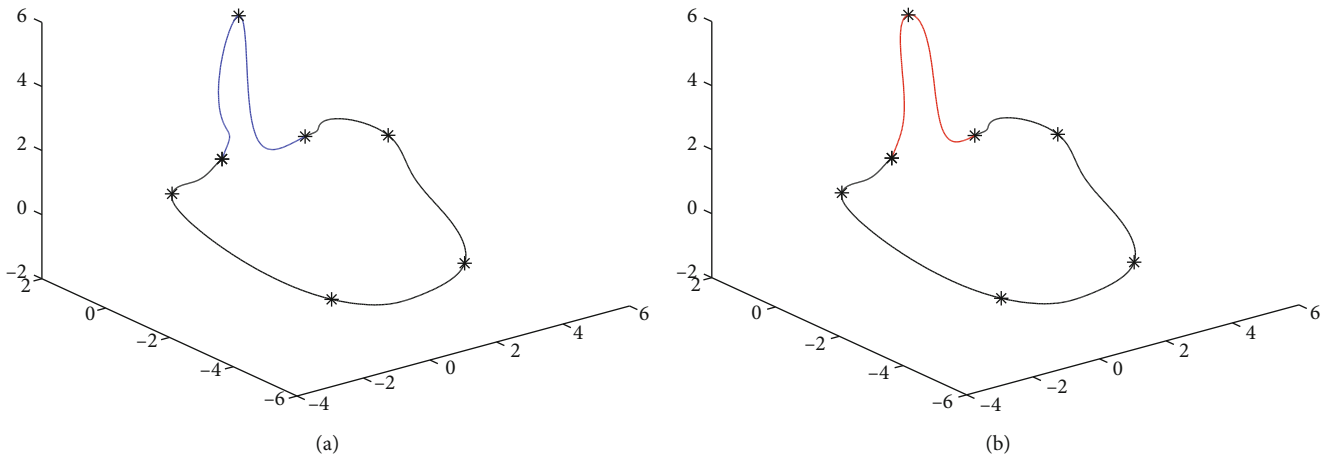

Figure 4: Local adjustment of spatial CTHI curve. (a) $(\alpha_i, \beta_i) = (1.5, 1.5)(i = 0, 1, \cdots, 5, 7)$, but $(\alpha_6, \beta_6) = (0.5, 2.5)$. (b) $(\alpha_i, \beta_i) = (1.5, 1.5)$ $(i = 0, 1, \cdots, 5, 7)$, but $(\alpha_6, \beta_6) = (1.5, 0.5)$.

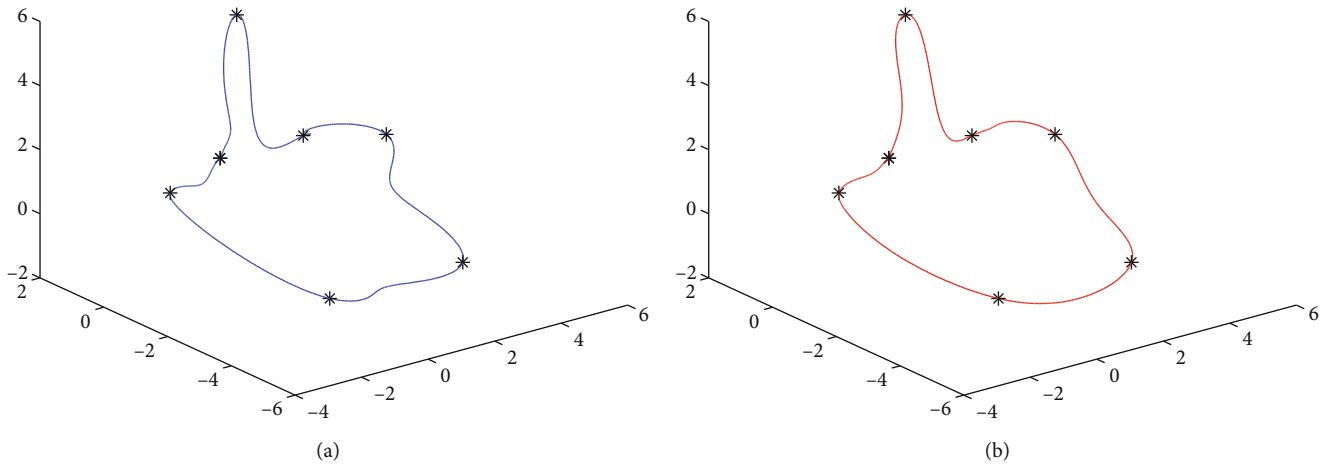

Figure 5: Global adjustment of spatial CTHI curve. (a) $(\alpha, \beta) = (1, 1.5)$. (b) $(\alpha, \beta) = (1.5, 1)$.

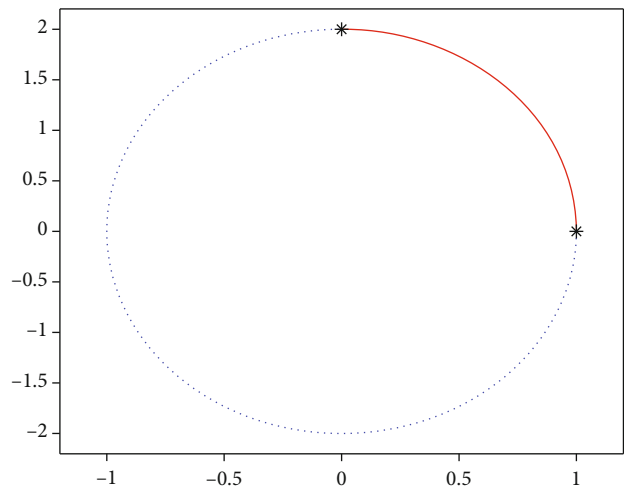

Figure 6: Accurate representation of an elliptical arc, where $a = 1$ and $b = 2$.

$\alpha_{i+1} = \beta_{i+1}$ in general, which cannot only maintain a certain degree of flexibility but also not make the operation too complicated. Then, the expression of CTHI curve can be described by

$$\begin{aligned} \boldsymbol{TH}_i(\alpha_i, \alpha_{i+1}; t) &= F_{i,0}(\alpha_i; t)\boldsymbol{p}_i + F_{i,1}(\alpha_{i+1}; t)\boldsymbol{p}_{i+1} \\ &\quad + G_{i,0}(\alpha_i; t)\boldsymbol{m}_i + G_{i,1}(\alpha_{i+1}; t)\boldsymbol{m}_{i+1}, \quad i = 0, 1, \cdots, n-1, \end{aligned} \tag{28}$$

where $0 \le t \le 1$, $\boldsymbol{p}_j$, and $\boldsymbol{m}_j (j = 0, 1, \cdots, n)$ are given points and corresponding tangent vectors, respectively, $F_{i,j}(\alpha_{i+j}; t)$ and $G_{i,j}(\alpha_{i+j}; t)(j = 0, 1)$ are expressed as

$$\begin{cases} F_{i,0}(\alpha_i; t) = (1 - \alpha_i) + 3(\alpha_i - 1)S^2 + 2(1 - \alpha_i)S^3 + \alpha_i C^3, \\ F_{i,1}(\alpha_{i+1}; t) = 2(\alpha_{i+1} - 1) + 3(1 - \alpha_{i+1})S^2 + \alpha_{i+1}S^3 + 2(1 - \alpha_{i+1})C^3, \\ G_{i,0}(\alpha_i; t) = -\alpha_i + S + (3\alpha_i - 2)S^2 + (1 - 2\alpha_i)S^3 + \alpha_i C^3, \\ G_{i,1}(\alpha_{i+1}; t) = \frac{1}{3}\left(2(3\alpha_{i+1} - 5) - 3C + 9(2 - \alpha_{i+1})S^2 + (3\alpha_{i+1} - 8)S^3 + (13 - 6\alpha_{i+1})C^3\right), \end{cases} \tag{29}$$

and $S \coloneqq \sin(t)$, $C \coloneqq \cos(t)$, $t \in [0, \pi/2]$, and $\alpha_i, \alpha_{i+1} \in R$.

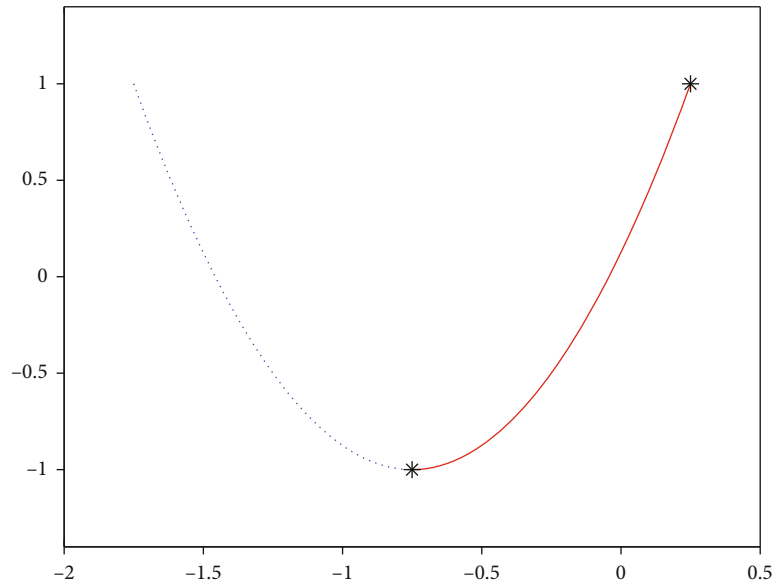

Figure 7: Accurate representation of a quadratic parabolic arc, where $a = 1$ and $b = 2$.

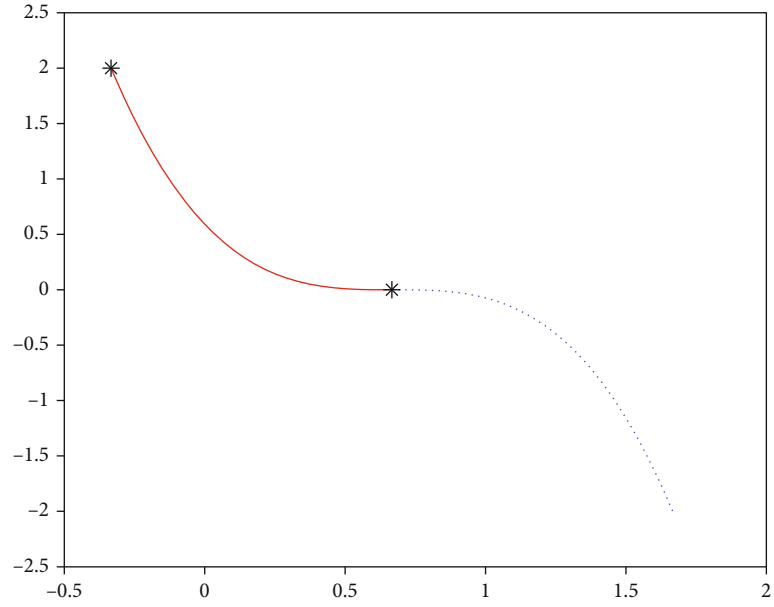

Figure 8: Accurate representation of a cubic parabolic arc, where $a = 1$ and $b = 2$.

Of course, we can adjust the shape of CTHI curve locally or globally by altering the values of α_i and α_{i+1} contained in each segment. However, it should also be noted that the shape of CTHI curve would be unsatisfactory if the free parameters are not selected properly.

Example 10. Given the same data as in Examples 4 and 5. Figure 10 shows CTHI curves with inappropriate free parameters.

In addition, sometimes people may need to determine the free parameters to make the shape of CTHI curve meet certain specific geometric requirements. Hence, we can give schemes for optimizing the free parameters according to some objectives. Because the internal energy minimization has been successfully used to optimize the shape of some parametric curves, we adopt it to optimize the shape of CTHI curve.

5.1. Shape Optimization of Planar CTHI Curve. Three types of commonly used internal energy of a planar curve are stretch energy, strain energy (also called bending energy), and curvature variation energy (often replaced by Jerk's energy). For a planar curve $\boldsymbol{b}(t)(a \le t \le b)$, its stretch energy, strain energy, and Jerk's energy are usually

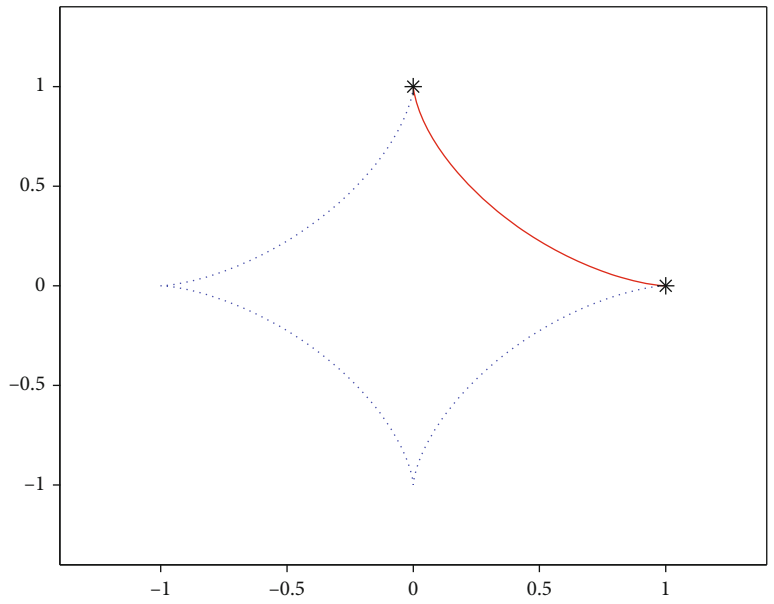

Figure 9: Accurate representation of an astroid arc, where $a = 1$.

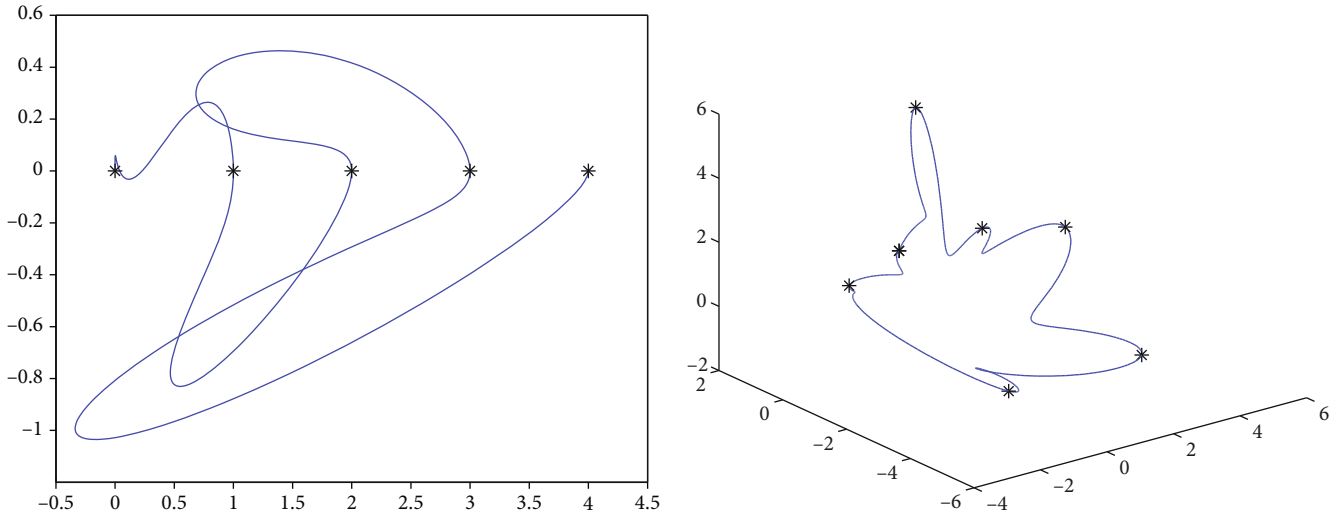

Figure 10: CTHI curves with inappropriate free parameters. (a) $(\alpha_0, \alpha_1, \cdots, \alpha_4) = (-2, 1, -1, 0, -3)$. (b) $\alpha_i = 0$, $i = 0, 1, \cdots, 7$.

approximately described by $\int_a^b \|\boldsymbol{b}'(t)\|^2 \mathrm{d}t$, $\int_a^b \|\boldsymbol{b}''(t)\|^2 \mathrm{d}t$ and $\int_a^b \|\boldsymbol{b}'''(t)\|^2 \mathrm{d}t$, respectively, see [20, 21]. Since CTHI curve expressed in Equation (28) is composed of n segments, we can define the internal energy of planar CTHI curve as follows.

Definition 11. Three types of internal energy of planar CTHI curve are approximately expressed as

$$E_k = \sum_{i=0}^{n-1} \int_0 \left\| \boldsymbol{TH}_i^{(k)}(\alpha_i, \alpha_{i+1}; t) \right\|^2 \mathrm{d}t, \; k = 1, 2, 3, \tag{30}$$

where $\boldsymbol{TH}_i^{(k)}(\alpha_i, \alpha_{i+1}; t)$ represents the kth derivative of $\boldsymbol{TH}_i(\alpha_i, \alpha_{i+1}; t)$ about t. Specifically, E_1, E_2 and E_3 is the stretch energy, the strain (or bend) energy, and the curvature variation (or Jerk's) energy of the curve, respectively.

From Equations (29), we can rewrite Equation (28) as

$$\boldsymbol{TH}_i(\alpha_i, \alpha_{i+1}; t) = \boldsymbol{A}_i(t)\alpha_i + \boldsymbol{B}_i(t)\alpha_{i+1} + \boldsymbol{C}_i(t), i = 0, 1, \cdots, n-1, \tag{31}$$

where

$$\boldsymbol{A}_i(t) := \left(-1 + 3S^2 - 2S^3 + C^3\right)(\boldsymbol{p}_i + \boldsymbol{m}_i)$$

$$\boldsymbol{B}_i(t) := \left(2 - 3S^2 + S^3 - 2C^3\right)(\boldsymbol{p}_{i+1} + \boldsymbol{m}_{i+1})$$

$$\boldsymbol{C}_i(t) \coloneqq \left(1-3S^2+2S^3\right)\boldsymbol{p}_i + \left(-2+3S^2+2C^3\right)\boldsymbol{p}_{i+1} + \left(S-2S^2+S^3\right)\boldsymbol{m}_i + \frac{1}{3}\left(-10-3C+18S^2-8S^3+13C^3\right)\boldsymbol{m}_{i+1},$$
$$S \coloneqq \sin(t), C \coloneqq \cos(t), \alpha_i, \alpha_{i+1} \in R. \quad (32)$$

By substituting Equation (31) into Equation (30) and by derivation, we obtain

$$E_k = \sum_{i=0}^{n-1}\left(a_{k,i}\alpha_i^2 + b_{k,i}\alpha_{i+1}^2 + c_{k,i} + 2d_{k,i}\alpha_i\alpha_{i+1} + 2e_{k,i}\alpha_i + 2f_{k,i}\alpha_{i+1}\right), \quad (33)$$

where

$a_{k,i} \coloneqq \int_0^{\pi/2}\|\boldsymbol{A}_i\ (k)(t)\|^{\ 2}\mathrm{d}t$, $b_{k,i} \coloneqq \int_0^{\pi/2}\|\boldsymbol{B}_i^{(k)}(t)\|^2\mathrm{d}t$, $c_{k,i} \coloneqq \int_0^{\pi/2}\|\boldsymbol{C}_i^{(k)}(t)\|^2\mathrm{d}t$,

$d_{k,i} \coloneqq \int_0\ \pi/2(\boldsymbol{A}_i^{(k)}(t)\ \cdot \boldsymbol{B}_i^{(k)}\ (t))\mathrm{d}t$, $e_{k,i} \coloneqq \int_0^{\pi/2}(\boldsymbol{A}_i^{(k)}(t)\cdot \boldsymbol{C}_i^{(k)}(t))dt$, $f_{k,i} \coloneqq \int_0^{\pi/2}(\boldsymbol{B}_i^{(k)}(t)\cdot \boldsymbol{C}_i^{(k)}(t))dt$.

Because $a_{k,i}$, $b_{k,i}$, $c_{k,i}$, $d_{k,i}$, $e_{k,i}$, $f_{k,i}$ are constants once $\boldsymbol{p}_{i+j}$, $\boldsymbol{m}_{i+j}(j=0,1)$ and k are selected, the internal energy expressed in Equation (33) are quadratic functions of α_i $(i=0,1,\cdots,n)$. Then, the following model can be gotten for generating planar CTHI curve with minimal internal energy,

$$\min_{\alpha_0,\alpha_1,\cdots,\alpha_n\in R} E_k(\alpha_0,\alpha_1,\cdots,\alpha_n), \quad (34)$$

where $k=1,2,3$.

From Equation (34), we have

$$\begin{cases} \dfrac{\partial E_k}{\partial \alpha_0} = 2a_{k,0}\alpha_0 + 2d_{k,0}\alpha_1 + 2e_{k,0}, \\ \dfrac{\partial E_k}{\partial \alpha_i} = 2d_{k,i-1}\alpha_{i-1} + 2(a_{k,i}+b_{k,i-1})\alpha_i + 2d_{k,i}\alpha_{i+1} + 2\left(e_{k,i}+f_{k,i-1}\right), \\ i=1,2,\cdots,n-1, \\ \dfrac{\partial E_k}{\partial \alpha_n} = 2d_{k,n-1}\alpha_{n-1} + 2b_{k,n-1}\alpha_n + 2f_{k,n-1}. \end{cases} \quad (35)$$

Since the solution of Equation (34) can be obtained by solving $\partial E_k/\partial\alpha_i = 0$, $i=0,1,\cdots,n$, from Equation (35), we get the following equation system,

$$\begin{cases} a_{k,0}\alpha_0 + d_{k,0}\alpha_1 = -e_{k,0}, \\ d_{k,i-1}\alpha_{i-1} + (a_{k,i}+b_{k,i-1})\alpha_i + d_{k,i}\alpha_{i+1} = -\left(e_{k,i}+f_{k,i-1}\right), \\ i=1,2,\cdots,n-1, \\ d_{k,n-1}\alpha_{n-1} + b_{k,n-1}\alpha_n = -f_{k,n-1}, \end{cases} \quad (36)$$

where $k=1,2,3$.

Let A_k be the coefficient matrix of Equation (36). It is clear that A_k is tridiagonal; then, the solution of Equation (36) can be easily obtained by using the LU method as long as A_k^{-1} exists for the given $\boldsymbol{p}_j$ and $\boldsymbol{m}_j(j=0,1,\cdots,n)$. Then, we can get the following theorem without proving.

Theorem 12. *For selected $k\,(k=1,2,3)$, suppose A_k^{-1} exists for the given $\boldsymbol{p}_j$ and $\boldsymbol{m}_j(j=0,1,\cdots,n)$, let $h_{k,0} \coloneqq -e_{k,0}$, $h_{k,j} \coloneqq -(e_{k,j}+f_{k,j-1})$, $j=1,2,\cdots,n-1$, $h_{k,n} \coloneqq -f_{k,n-1}$, $(g_{i,j}^k) \coloneqq A_k^{-1}$; the solution of Equation (34), denoted by $\alpha_{k,i}$, $i=0,1,2,\cdots,n$, is expressed as*

$$\alpha_{k,i} = \sum_{j=0}^{n} g_{i,j}^k h_{k,j},\ i=0,1,2,\cdots,n. \quad (37)$$

Example 13. Given

$\boldsymbol{p}_0=(1,2)$, $\boldsymbol{p}_1=(3,4)$, $\boldsymbol{p}_2=(5,2)$, $\boldsymbol{p}_3=(7,4)$, $\boldsymbol{p}_4=(9,2)$, $\boldsymbol{m}_0=(1,2)$, $\boldsymbol{m}_1=(-4,0)$, $\boldsymbol{m}_2=(2,0)$, $\boldsymbol{m}_3=(-4,0)$, $\boldsymbol{m}_4=(1,2)$.

The corresponding CTHI curve is composed of four segments. By computing from Equation (37), the optimal free parameters can be obtained as follows:

(a) Stretch energy minimization ($viz.k=1$),

$$(\alpha_{1,0},\alpha_{1,1},\cdots,\alpha_{1,4}) = (1.3955,1.3959,2.1150,1.7660,2.3859) \quad (38)$$

(b) Strain energy minimization ($viz.k=2$),

$$(\alpha_{2,0},\alpha_{2,1},\cdots,\alpha_{2,4}) = (1.8858,1.6040,1.9430,2.1402,1.8706) \quad (39)$$

(c) Curvature variation energy minimization ($viz.k=3$),

$$(\alpha_{3,0},\alpha_{3,1},\cdots,\alpha_{3,4}) = (1.8262,1.5796,1.7821,1.9774,1.5931) \quad (40)$$

The CTHI curves generated by taking inappropriate free parameters and minimizing the internal energy are shown in Figure 11.

Example 14. Given $\boldsymbol{p}_0=(0,0)$, $\boldsymbol{p}_1=(3,1)$, $\boldsymbol{p}_2=(5,2)$, $\boldsymbol{p}_3=(6,4)$, $\boldsymbol{p}_4=(8,5)$, $\boldsymbol{p}_5=(11,6)$, $\boldsymbol{m}_0=(0.8,1.5)$, $\boldsymbol{m}_1=(3.5,0.9)$, $\boldsymbol{m}_2=(0.9,0.6)$, $\boldsymbol{m}_3=(1.6,1.0)$, $\boldsymbol{m}_4=(1.3,1.3)$, and $\boldsymbol{m}_5=(4.9,1.3)$.

The corresponding CTHI curve is composed of five segments. By computing from Equation (37), the optimal free parameters can be obtained as follows:

(a) Stretch energy minimization ($viz.k=1$),

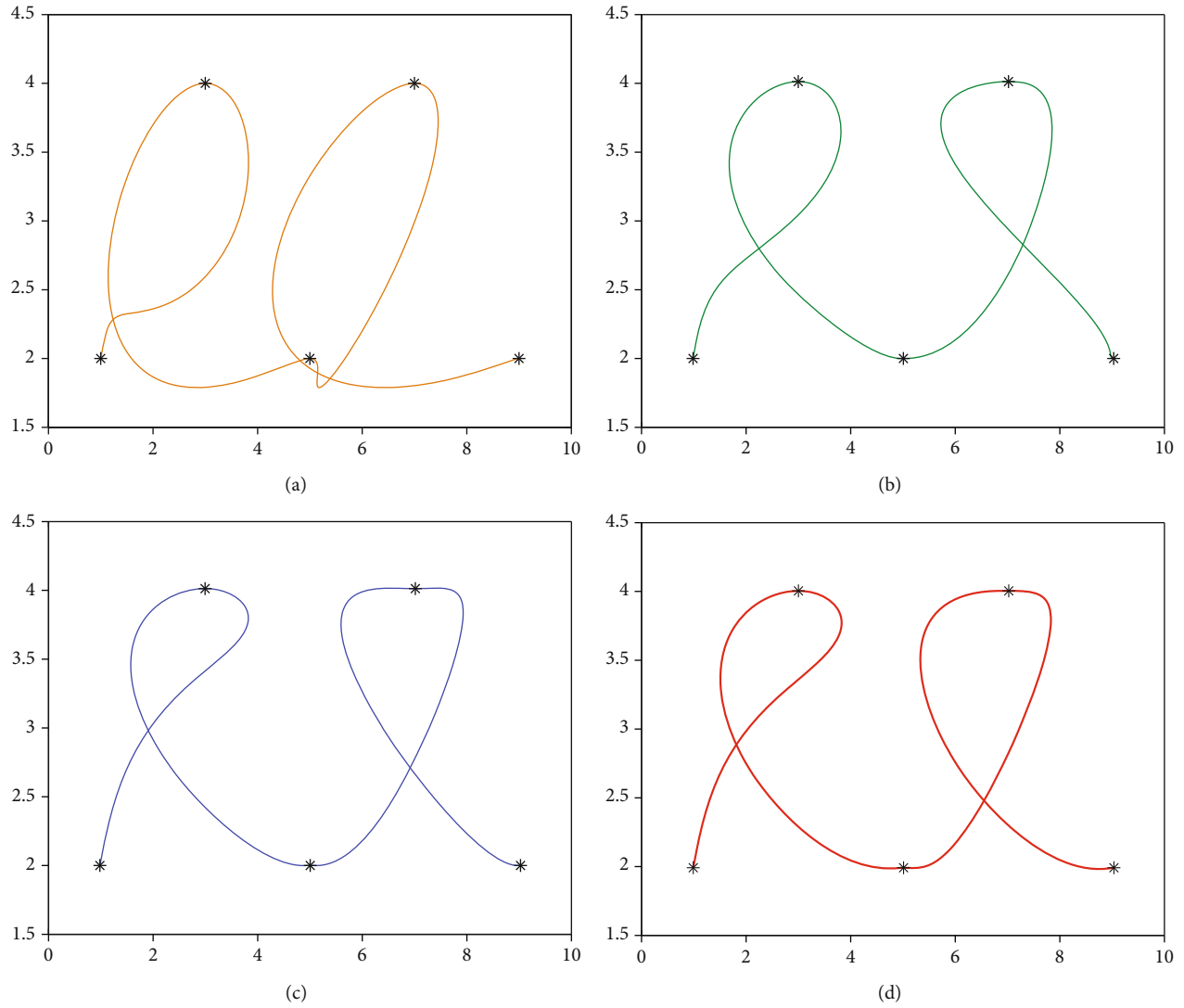

FIGURE 11: The CTHI curves generated in Example 13. (a) Taking inappropriate free parameters $\alpha_i = 1$, $i = 0, 1, \cdots, 4$. (b) Stretch energy minimization. (c) Strain energy minimization. (d) Curvature variation energy minimization.

$$(\alpha_{1,0}, \alpha_{1,1}, \cdots, \alpha_{1,5}) = (1.4738, 1.6062, 1.7669, 1.9381, 1.8368, 2.1508) \tag{41}$$

(b) Strain energy minimization ($viz.k = 2$),

$$(\alpha_{2,0}, \alpha_{2,1}, \cdots, \alpha_{2,5}) = (1.1326, 1.6069, 1.8997, 1.8654, 1.8644, 1.9352) \tag{42}$$

(c) Curvature variation energy minimization ($viz.k = 3$),

$$(\alpha_{3,0}, \alpha_{3,1}, \cdots, \alpha_{3,5}) = (0.8390, 1.5787, 1.9148, 1.8552, 1.8832, 1.9413) \tag{43}$$

The CTHI curves generated by taking inappropriate free parameters and minimizing the internal energy are shown in Figure 12.

Example 15. Let us consider the following data taken from a unit circle,

$\boldsymbol{p}_i = (\cos(t_i), \sin(t_i))$, $\boldsymbol{m}_i = (-\sin(t_i), \cos(t_i))$, $t_i = i\pi/3$, $i = 0, 1, \cdots, 6$.

The corresponding CTHI curve is composed of six segments. By computing from Equation (37), the optimal free parameters can be obtained as follows,

(a) Stretch energy minimization ($viz.k = 1$),

$$(\alpha_{1,0}, \alpha_{1,1}, \cdots, \alpha_{1,6}) = (1.0435, 1.3575, 1.3140, 1.3192, 1.3244, 1.2809, 1.5949) \tag{44}$$

(b) Strain energy minimization ($viz.k = 2$),

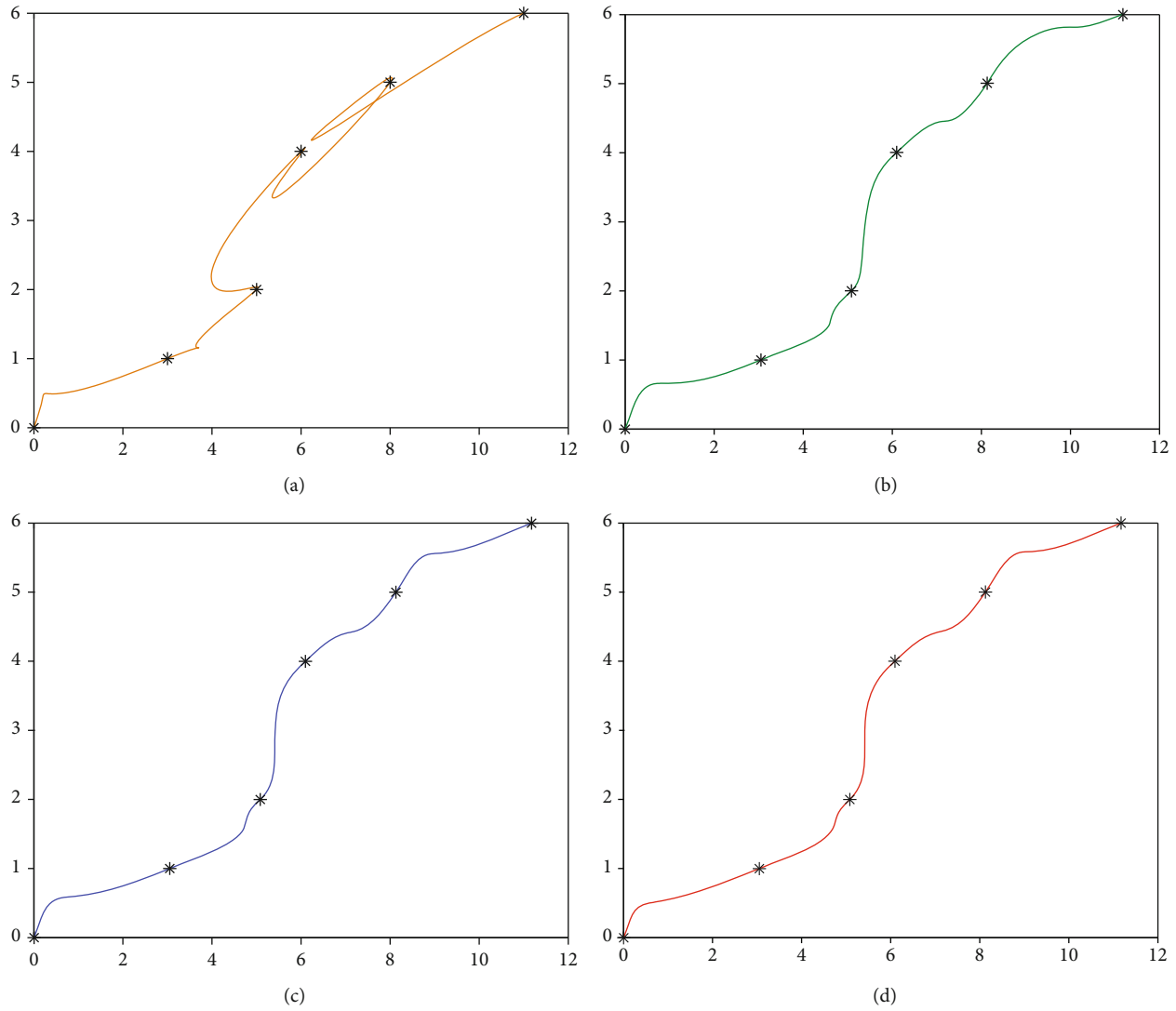

FIGURE 12: The CTHI curves generated in Example 14. (a) Taking inappropriate free parameters $\alpha_i = 1.2$, $i = 0, 1, \cdots, 5$. (b) Stretch energy minimization. (c) Strain energy minimization. (d) Curvature variation energy minimization.

$$(\alpha_{2,0}, \alpha_{2,1}, \cdots, \alpha_{2,6}) = (1.5268, 1.6235, 1.6179, 1.6182, 1.6185, 1.6130, 1.7097) \tag{45}$$

(c) Curvature variation energy minimization (*viz.*$k = 3$),

$$(\alpha_{3,0}, \alpha_{3,1}, \cdots, \alpha_{3,6}) = (1.4231, 1.6655, 1.6836, 1.6851, 1.6866, 1.7048, 1.9471) \tag{46}$$

The CTHI curves (solid lines) generated by taking inappropriate free parameters and minimizing the internal energy and the unit circle (dotted lines) are shown in Figure 13.

Figures 11–13 show that planar CTHI curves generated by the internal energy minimization are satisfactory compared with the curves whose free parameters are not appropriate.

5.2. Shape Optimization of Spatial CTHI Curve. As we know, planar curves only need to consider bending, while spatial curves should consider not only bending but also twisting. For a spatial curve $\boldsymbol{b}(t)(a \le t \le b)$, its bending energy and twisting energy can be described by [20]

$$E_{\text{bend}} = \int_a^b \kappa^2(t) \left\| \boldsymbol{b}'(t) \right\|^2 dt, E_{\text{twist}} = \int_a^b \tau^2(t) \left\| \boldsymbol{b}'(t) \right\|^2 dt, \tag{47}$$

where $\kappa(t)$ and $\tau(t)$ represents the curvature and the torsion of the curve, respectively.

To facilitate the calculation, Equation (47) can be approximately described by [20]

$$\widehat{E}_{\text{bend}} = \int_a^b \left\| \boldsymbol{b}''(t) \right\|^2 dt, \widehat{E}_{\text{twist}} = \int_a^b \left\| \boldsymbol{b}'''(t) \right\|^2 dt. \tag{48}$$

It should be noted that Equation (48) is regarded as

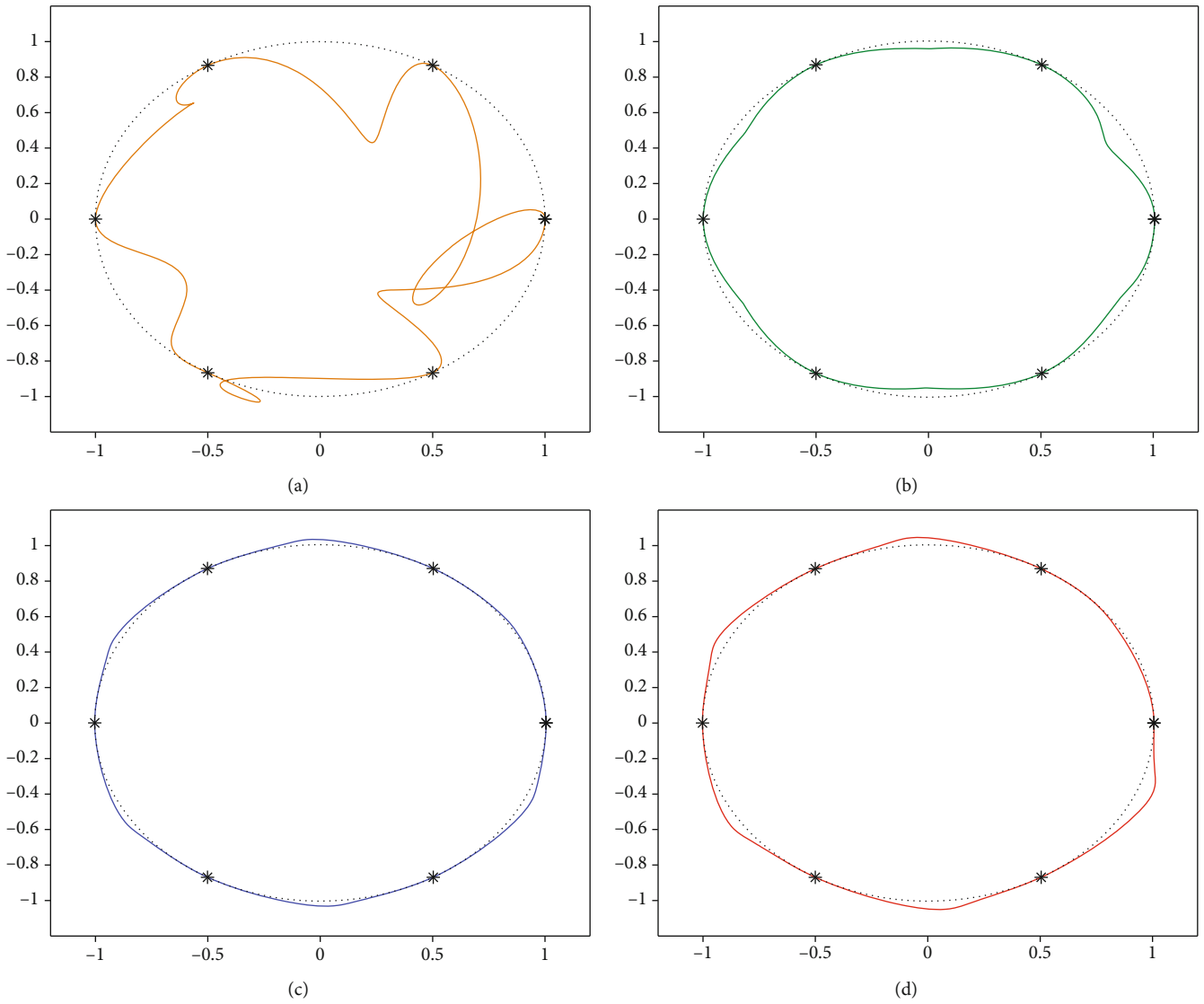

FIGURE 13: The CTHI curves generated in example 15. (a) Taking inappropriate free parameters $(\alpha_0, \alpha_1, \cdots, \alpha_6) = (-2, -1, 1, 0, 2, -1, 1)$. (b) Stretch energy minimization. (c) Strain energy minimization. (d) Curvature variation energy minimization.

approximate bending energy (or strain energy) and curvature variation energy (or Jerk's energy) of planar curves. Here, Equation (48) is adopted to describe the approximate bending energy and twisting energy of spatial curves. According to Definition 1, the blending energy and the twisting energy of CTHI curve can be approximately expressed as E_2 and E_3, respectively. Since spatial CTHI curve should consider bending and twisting at the same time, we can define the internal energy of spatial CTHI curve as follows.

Definition 16. The internal energy of spatial CTHI curve is approximately expressed as

$$E = \lambda E_2 + (1 - \lambda) E_3, \tag{49}$$

where $\lambda (0 < \lambda < 1)$ is the weight, and

$$\begin{aligned} E_2 &= \sum_{i=0}^{n-1} \int_0^{\pi/2} \left\| \boldsymbol{TH}_i''(\alpha_i, \alpha_{i+1}; t) \right\|^2 dt, \\ E_3 &= \sum_{i=0}^{n-1} \int_0^{\pi/2} \left\| \boldsymbol{TH}_i'''(\alpha_i, \alpha_{i+1}; t) \right\|^2 dt. \end{aligned} \tag{50}$$

From Equation (33), we can find that the energy expressed in Equation (49) is a quadratic function of $\alpha_i (i = 0, 1, \cdots, n)$. Then, we can obtain the following model for generating spatial CTHI curve with minimal internal energy,

$$\min_{\alpha_0, \alpha_1, \cdots, \alpha_n \in R} E(\alpha_0, \alpha_1, \cdots, \alpha_n) = \lambda E_2(\alpha_0, \alpha_1, \cdots, \alpha_n) + (1 - \lambda) E_3(\alpha_0, \alpha_1, \cdots, \alpha_n). \tag{51}$$

Before solving Equation (51), the value of λ needs to be selected. Here, we use the sorting algorithm [29] to select the value of λ, which is described in Algorithm 1.

Step 1: compute the deviations between the bending energy E_2 and the twisting energy E_3, that is,
$\delta_1 = E_2(\alpha_{3,0}, \alpha_{3,1},\cdots,\alpha_{3,n}) - E_2(\alpha_{2,0}, \alpha_{2,1},\cdots,\alpha_{2,n})$,
$\delta_2 = E_3(\alpha_{2,0}, \alpha_{2,1},\cdots,\alpha_{2,n}) - E_3(\alpha_{3,0}, \alpha_{3,1},\cdots,\alpha_{3,n})$,
where $\alpha_{k,i}$, $k = 2, 3$, $i = 0, 1, 2, \cdots, n$ are obtained by Equation (37).
Step 2: compute the initial weights of the bending energy E_2 and the twisting energy E_3, that is, $\lambda_1 = \delta_1/(\delta_1 + \delta_2)$, $\lambda_2 = \delta_2/(\delta_1 + \delta_2)$.
Step 3: if $\lambda_1 \geq \lambda_2$, the weight is taken as $\lambda = \lambda_2$; else, the weight is taken as $\lambda = \lambda_1$.

Algorithm 1: Determining the value of weight λ in Equation (51).

Then, according to Equations (35) and (49), we have

$$\begin{cases} \dfrac{\partial E}{\partial \alpha_0} = 2(\lambda a_{2,0} + (1-\lambda)a_{3,0})\alpha_0 + 2(\lambda d_{2,0} + (1-\lambda)d_{3,0})\alpha_1 + 2(\lambda e_{2,0} + (1-\lambda)e_{3,0}), \\ \dfrac{\partial E}{\partial \alpha_i} = 2(\lambda d_{2,i-1} + (1-\lambda)d_{3,i-1})\alpha_{i-1} + 2(\lambda(a_{2,i} + b_{2,i-1}) + (1-\lambda)(a_{3,i} + b_{3,i-1}))\alpha_i + 2(\lambda d_{2,i} + (1-\lambda)d_{3,i})\alpha_{i+1} + 2\big(\lambda\big(e_{2,i} + f_{2,i-1}\big) + (1-\lambda)\big(e_{3,i} + f_{3,i-1}\big)\big), \\ i = 1, 2, \cdots, n-1, \\ \dfrac{\partial E}{\partial \alpha_n} = 2(\lambda d_{2,n-1} + (1-\lambda)d_{3,n-1})\alpha_{n-1} + 2(\lambda b_{2,n-1} + (1-\lambda)b_{3,n-1})\alpha_n + 2\big(\lambda f_{2,n-1} + (1-\lambda)f_{3,n-1}\big). \end{cases} \tag{52}$$

Since the solution of Equation (51) can be obtained by solving $\partial E/\partial \alpha_i = 0$, $i = 0, 1, \cdots, n$, from Equation (52), we get the following equation system,

$$\begin{cases} (\lambda a_{2,0} + (1-\lambda)a_{3,0})\alpha_0 + (\lambda d_{2,0} + (1-\lambda)d_{3,0})\alpha_1 = -(\lambda e_{2,0} + (1-\lambda)e_{3,0}), \\ (\lambda d_{2,i-1} + (1-\lambda)d_{3,i-1})\alpha_{i-1} + (\lambda(a_{2,i} + b_{2,i-1}) + (1-\lambda)(a_{3,i} + b_{3,i-1}))\alpha_i + (\lambda d_{2,i} + (1-\lambda)d_{3,i})\alpha_{i+1} = -\big(\lambda\big(e_{2,i} + f_{2,i-1}\big) + (1-\lambda)\big(e_{3,i} + f_{3,i-1}\big)\big), \\ i = 1, 2, \cdots, n-1, \\ (\lambda d_{2,n-1} + (1-\lambda)d_{3,n-1})\alpha_{n-1} + (\lambda b_{2,n-1} + (1-\lambda)b_{3,n-1})\alpha_n = -\big(\lambda f_{2,n-1} + (1-\lambda)f_{3,n-1}\big). \end{cases} \tag{53}$$

Let B be the coefficient matrix of Equation (53). It is clear that B is tridiagonal; then, the solution of Equation (53) can be easily obtained by using the LU method as long as B^{-1} exists for the given $\boldsymbol{p}_j$ and $\boldsymbol{m}_j (j = 0, 1,\cdots,n)$. Then, we can get the following theorem without proving.

Theorem 17. *Suppose B^{-1} exists for the given $\boldsymbol{p}_j$ and $\boldsymbol{m}_j (j = 0, 1,\cdots,n)$, let*

$s_0 := -(\lambda e_{2,0} + (1-\lambda)\, e_{3,0})$, $s_j := -(\lambda(e_{2,j} + f_{2,j-1}) + (1-\lambda)(e_{3,j} + f_{3,j-1}))$, $j = 1, 2, \cdots, n-1$,
$s_n := -(\lambda f_{2,n-1} + (1-\lambda)f_{3,n-1})$, $(r_{i,j}) := B^{-1}$.
The solution of Equation (51) is expressed as

$$\alpha_i = \sum_{j=0}^{n} r_{i,j} s_j, \; i = 0, 1, 2, \cdots, n. \tag{54}$$

Example 18. Let us consider the following data taken from a cylindrical spiral, $p_i = (\cos(t_i), \sin(t_i), 2t_i)$, $m_i = (-\sin(t_i), \cos(t_i), 2)$, $t = i\pi/2$, $i = 0, 1, 2, 3, 4$.

The corresponding CTHI curve is composed of four segments. By computing from Equation (54), the optimal free parameters of CTHI curve with minimal internal energy are

$$(\alpha_0, \alpha_1,\cdots,\alpha_4) = (1.4215, 1.4992, 1.4992, 1.4992, 1.5768). \tag{55}$$

The CTHI curves (solid lines) generated by taking inappropriate free parameters and minimizing the internal energy and the cylindrical spiral (dotted lines) are shown in Figure 14.

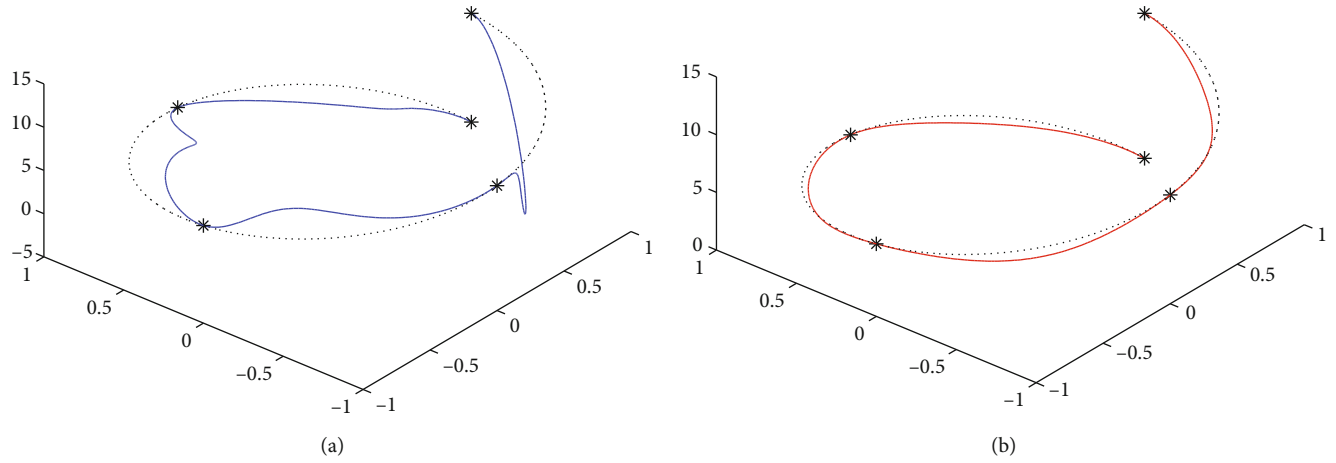

FIGURE 14: The CTHI curves generated in Example 18. (a) Taking inappropriate free parameters $(\alpha_0, \alpha_1, \cdots, \alpha_4) = (1, 0, -2, 1, -1)$. (b) Internal energy minimization.

Figure 14 shows that spatial CTHI curve generated by minimizing the internal energy is satisfactory compared with the curve with inappropriate free parameters.

6. Conclusion

We first proposed a cubic trigonometric Hermite interpolation curve in this paper. Different from cubic Hermite interpolation curve, the proposed curve achieves C^2 continuity, has local and global adjustability, and can accurately represent some engineering curves. These features are very conducive to geometric modeling. To generate the trigonometric Hermite interpolation curve with specific shapes, the schemes for determining the optimal values of the free parameters based on internal energy minimization are presented. The planar curves and spatial curves with minimal internal energy are satisfactory compared with the curves with inappropriate free parameters. In contrast to cubic Hermite interpolation curve, the cubic trigonometric Hermite interpolation curve is more practical in geometric modeling.

Data Availability

All the data used for the numerical analysis are mentioned within the article.

Conflicts of Interest

The authors declare that there are no conflicts of interest.

Acknowledgments

This work was supported by the Hunan Provincial Natural Science Foundation of China under Grant No. 2021JJ30373, and the National Natural Science Foundation of China under Grant No. 12101225.

References

[1] G. Farin, *Curves and Surfaces for CAGD: A Practical Guide*, Academic Press, 2002.

[2] C. Rabbath and D. Corriveau, "A comparison of piecewise cubic Hermite interpolating polynomials, cubic splines and piecewise linear functions for the approximation of projectile aerodynamics," *Defence Technology*, vol. 15, no. 5, pp. 741–757, 2019.

[3] S. Shang and S. Shang, "Estimating gini coefficient from grouped data based on shape-preserving cubic Hermite interpolation of Lorenz curve," *Mathematics*, vol. 9, no. 20, p. 2551, 2021.

[4] X. Zhang, Y. Huo, and D. Wan, "Improved EMD based on piecewise cubic Hermite interpolation and mirror extension," *Chinese Journal of Electronics*, vol. 29, no. 5, pp. 899–905, 2020.

[5] O. Tamin, B. Ikram, A. Ramli, E. Moung, and C. Yee, "Travel-time estimation by cubic Hermite curve," *Information*, vol. 13, no. 7, p. 307, 2022.

[6] J. Merrien and P. Sablonnière, "Rational splines for Hermite interpolation with shape constraints," *Computer Aided Geometric Design*, vol. 30, no. 3, pp. 296–309, 2013.

[7] U. Bashir, M. Abba, and J. Ali, "The G^2 and C^2 rational quadratic trigonometric Bezier curve with two shape parameters with applications," *Applied Mathematics and Computation*, vol. 219, no. 20, pp. 10183–10197, 2013.

[8] J. Li, "A class of quintic Hermite interpolation curve and the free parameters selection," *Journal of Advanced Mechanical Design, Systems, and Manufacturing*, vol. 13, no. 1, 2019.

[9] J. Xie and X. Liu, "Adjustable piecewise quartic Hermite spline curve with parameters," *Mathematical Problems in Engineering*, vol. 2021, Article ID 2264871, 6 pages, 2021.

[10] J. Zheng, G. Hu, X. Ji, and X. Qin, "Quintic generalized Hermite interpolation curves: construction and shape optimization using an improved GWO algorithm," *Computational and Applied Mathematics*, vol. 41, no. 3, p. 115, 2022.

[11] X. Tan and Y. Zhu, "Quasi-quintic trigonometric Bézier curves with two shape parameters," *Computational and Applied Mathematics*, vol. 38, no. 4, p. 157, 2019.

[12] S. Maqsood, M. Abbas, G. Hu, A. Ramli, and K. Miura, "A novel generalization of trigonometric Bézier curve and surface

with shape parameters and its applications," *Mathematical Problems in Engineering*, vol. 2020, Article ID 4036434, 25 pages, 2020.

[13] S. Naseer, M. Abbas, H. Emadifar, S. Bibi, T. Nazir, and Z. Shah, "A class of sextic trigonometric Bézier curve with two shape parameters," *Journal of Mathematics*, vol. 2021, Article ID 9989810, 16 pages, 2021.

[14] M. Ameer, M. Abbas, T. Abdeljawad, and T. Nazir, "A novel generalization of Bézier-like curves and surfaces with shape parameters," *Mathematics*, vol. 10, no. 3, p. 376, 2022.

[15] X. Han, "Normalized B-basis of the space of trigonometric polynomials and curve design," *Applied Mathematics and Computation*, vol. 251, pp. 336–348, 2015.

[16] L. Yan, "Cubic trigonometric nonuniform spline curves and surfaces," *Mathematical Problems in Engineering*, vol. 2016, Article ID 7067408, 9 pages, 2016.

[17] S. Samreen, M. Sarfraz, and A. Mohamed, "A quadratic trigonometric B-spline as an alternate to cubic B-spline," *Alexandria Engineering Journal*, vol. 61, no. 12, pp. 11433–11443, 2022.

[18] J. Li, L. Song, and C. Liu, "The cubic trigonometric automatic interpolation spline," *IEEE/CAA Journal of Automatica Sinica*, vol. 5, no. 6, pp. 1136–1141, 2018.

[19] J. Li, "A class of cubic trigonometric automatic interpolation curves and surfaces with parameters," *Mathematical and Computational Applications*, vol. 21, no. 2, p. 18, 2016.

[20] R. Veltkamp and W. Wesselink, "Modeling 3D curves of minimal energy," *Computer Graphics Forum*, vol. 14, no. 3, pp. 97–110, 1995.

[21] G. Xu, G. Wang, and W. Chen, "Geometric construction of energy-minimizing Béezier curves," *Science China-Information Sciences*, vol. 54, no. 7, pp. 1395–1406, 2011.

[22] Y. Ahn, C. Hoffmann, and P. Rosen, "Geometric constraints on quadratic Bezier curves using minimal length and energy," *Journal of Computational and Applied Mathematics*, vol. 255, pp. 887–897, 2014.

[23] L. Lu, "A note on curvature variation minimizing cubic Hermite interpolants," *Applied Mathematics and Computation*, vol. 259, pp. 596–599, 2015.

[24] H. Eriskin and A. Yücesan, "Bézier curve with a minimal jerk energy," *Mathematical Sciences and Applications E-Notes*, vol. 4, no. 2, pp. 139–148, 2016.

[25] L. Lu, C. Jiang, and Q. Hu, "Planar cubic G^1 and quintic G^2 Hermite interpolations via curvature variation minimization," *Computers & Graphics*, vol. 70, pp. 92–98, 2017.

[26] G. Xu, Y. Zhu, L. Deng, G. Wang, B. Li, and K. Hui, "Efficient construction of B-spline curves with minimal internal energy," *CMC-Computers Materials & Continua*, vol. 58, no. 3, pp. 879–892, 2019.

[27] J. Li and L. Zhang, "Length and curvature variation energy minimizing planar cubic G^1 Hermite interpolation curve," *Journal of Taibah University for Science*, vol. 14, no. 1, pp. 60–64, 2020.

[28] J. Li, C. Liu, and S. Liu, "The quartic Catmull–Rom spline with local adjustability and its shape optimization," *Advances in Continuous and Discrete Models*, vol. 2022, no. 1, p. 59, 2022.

[29] C. Lin and J. Dong, *The Methods and Theories of Multi-Objective Optimizations*, Jilin Education Press, 1992.